



1 **Wintertime New Particle Formation and Its Contribution to Cloud Condensation**  
2 **Nuclei in the Northeastern United States**

3 Fangqun Yu<sup>1</sup>, Gan Luo<sup>1</sup>, Arshad Nair<sup>1</sup>, James J. Schwab<sup>1</sup>, James P. Sherman<sup>2</sup>, and Yanda Zhang<sup>1</sup>

4 <sup>1</sup>Atmospheric Sciences Research Center, State University of New York, Albany, New York 12203, USA

5 <sup>2</sup>Department of Physics and Astronomy, Appalachian State University, NC 28608, USA

6 **Abstract:** Atmospheric particles can act as cloud condensation nuclei (CCN) and modify cloud  
7 properties and precipitation and thus indirectly impact the hydrological cycle and climate. New  
8 particle formation (NPF or nucleation), frequently observed at locations around the globe, is an  
9 important source of ultrafine particles and CCN in the atmosphere. In this study, wintertime NPF  
10 over the Northeastern United States (NEUS) is simulated with WRF-Chem coupled with a size-  
11 resolved (sectional) advanced particle microphysics (APM) model. Model simulated variations of  
12 particle number concentrations during a two-month period (November–December 2013) are in  
13 agreement with corresponding measurements taken at Pinnacle State Park (PSP), New York and  
14 Appalachian State University (APP), North Carolina. We show that even during wintertime,  
15 regional nucleation occurs and contributes significantly to ultrafine particle and CCN number  
16 concentrations over the NEUS. Due to low biogenic emissions during this period, wintertime  
17 regional nucleation is solely controlled by inorganic species and the newly developed ternary ion-  
18 mediated nucleation scheme is able to capture the variations of observed particle number  
19 concentrations (ranging from  $\sim 200 - 20,000 \text{ cm}^{-3}$ ) at both PSP and APP. Total particle and CCN  
20 number concentrations dramatically increase following NPF events and have highest values over  
21 the Ohio Valley region, where elevated  $[\text{SO}_2]$  is sustained by power plants. Secondary particles  
22 dominate particle number abundance over the NEUS and their fraction increases with altitude  
23 from  $>85\%$  near surface to  $>95\%$  in the upper troposphere. The secondary fraction of CCN also  
24 increases with altitude, from 20–50% in the lower boundary layer to 50–60% in the middle  
25 troposphere to 70–85% in the upper troposphere. This significant contribution of wintertime  
26 nucleation to aerosols, especially those that can act as CCN, is important considering the changing  
27 paradigm of wintertime precipitation over the NEUS.

28



## 29 1. Introduction

30 Particle number concentration is a key parameter important for the health and climate impacts  
31 of atmospheric aerosols. High number concentrations of ultrafine particles may lead to adverse  
32 health effects (Knibbs et al., 2011; Han et al., 2016). Variations in the number concentration of  
33 cloud condensation nuclei (CCN) influence cloud properties and precipitation and thus indirectly  
34 affect the hydrological cycle and climate (e. g, Twomey, 1977; Charlson et al., 1992). Aerosol  
35 particles appear in the troposphere due to either in-situ new particle formation (NPF, i.e, formation  
36 of secondary particles (SP) via nucleation) or direct emissions (i.e., primary particles (PP)).  
37 Though NPF has little effect on the total particle mass in the immediate vicinity of the nucleation  
38 itself, it is highly relevant to the aerosol health and climate effects as SP can dominate the ultrafine  
39 particles and those particles that can act as CCN (Spracklen et al., 2008; Pierce and Adams, 2009;  
40 Yu and Luo, 2009). Aerosol number concentrations exhibit significant spatial and temporal  
41 variability due to non-linear dependence of NPF rates on atmospheric conditions and  
42 concentrations of gaseous precursors, both of which are subject to changes as a result of climate  
43 changes and emission regulatory actions.

44 Laboratory experiments and theoretical studies indicate that sulfuric acid, ammonia, amines,  
45 ions, and certain organic compounds can all contribute to NPF (see recent review paper by Lee et  
46 al., 2019). However, the actual contribution of various nucleation pathways and key controlling  
47 parameters in the real atmosphere remains elusive, especially with regard to the relative  
48 importance of inorganic versus organic nucleation (e.g., Yu et al., 2015). Inorganic and organic  
49 nucleation precursors have quite different sources and their emission strengths depend on different  
50 factors, with important implications to spatial distributions of NPF and CCN and their short-term  
51 (diurnal, seasonal) and long-term (pre-industry, present, and future climate and emissions)  
52 variations. Both inorganic and organic nucleation schemes are subject to uncertainties and it is  
53 important to evaluate their ability to capture particle formation and variations of number  
54 concentration in the atmosphere. Yu et al. (2015) showed that both inorganic nucleation and  
55 organic mediated nucleation can explain NPF observed in a spring month at several forest sites in  
56 North America but organic-mediated nucleation over-predicted NPF in the summer.

57 The main objective of the present study is to investigate the new particle formation process  
58 and its contribution to particle number concentration and CCN in the wintertime in the  
59 Northeastern United States (NEUS). Wintertime biogenic emissions are very low in NEUS and



60 thus the contribution of biogenic organic species to NPF is expected to be negligible, enabling us  
61 to unequivocally evaluate the performance of the inorganic nucleation scheme. In addition to  
62 delineating the underlying processes controlling particle number concentrations in the  
63 atmosphere, an improved understanding of major sources and concentrations of CCN in  
64 wintertime is also important for better forecasting wintertime precipitation, such as snow storms,  
65 in NEUS (Gaudet et al., 2019).

66

## 67 **2. Methods**

### 68 2.1 Model

69 We employ WRF-Chem (version 3.7.1), a regional multi-scale meteorology model coupled  
70 with online chemistry (Grell et al., 2005). The model configurations include Morrison 2-mom  
71 microphysics (Morrison et al., 2009), RRTMG longwave and shortwave radiation (Clough et al.,  
72 2005), Noah land surface, Grell-3 cumulus (Grell and Freitas, 2014), and YSU PBL scheme (Hong  
73 et al., 2006). We use CB05 scheme (Yarwood et al., 2005) for gas-phase chemistry, SORGAM  
74 with aqueous reactions (Schell et al., 2001) for secondary organic aerosol chemistry and aqueous  
75 phase chemistry, and ISORROPIA II (Fountoukis and Nenes, 2007) for aerosol thermodynamic  
76 equilibrium. The initial and boundary conditions for meteorology are generated from the National  
77 Centers for Environmental Prediction (NCEP) Final (FNL) with resolution at  $1^\circ \times 1^\circ$  and time  
78 intervals at six hours. The anthropogenic emissions are based on the Environmental Protection  
79 Agency's (EPA) National Emission Inventory (NEI) 2011, and the biogenic emissions are  
80 calculated using MEGAN (Guenther et al., 2006). Annual scaling factors for NO<sub>x</sub>, SO<sub>2</sub>, NH<sub>3</sub>, and  
81 CO derived from EPA's Air Pollutant Emissions Trends Data from 1990 to 2016 are used here to  
82 scale the emissions of corresponding species from the baseline year of 2011 to the simulation year.  
83 We also considered seasonal variation of NH<sub>3</sub> emission due to agricultural activity in the model.

84 For particle microphysics, we use a size-resolved (sectional) advanced particle microphysics  
85 (APM) model (Yu and Luo, 2009) that was previously integrated into WRF-Chem v3.1.1 (Luo and  
86 Yu, 2011). For this study, we have updated APM and integrated it into WRF-Chem v3.7.1. Major  
87 changes to APM include: (1) employment of 15 bins to represent black carbon (BC) and another  
88 15 bins to represent primary organic carbon (POC) particles in the size range of 3 nm to 2  $\mu$ m  
89 (instead of two log-normal modes in the previous version); (2) consideration of the successive  
90 oxidation aging of secondary organic gases (SOG) and explicit kinetic condensation of low volatile



91 SOG onto particles following the scheme of Yu (2011); (3) fully coupled APM aerosols with WRF-  
92 Chem radiation code and cloud microphysics, with aerosol optical properties and aerosol activation  
93 calculated from size-resolved APM aerosols using optical properties lookup tables (Yu et al., 2012)  
94 and the activation scheme of Abdul-Razzak and Ghan (2002). Cloud droplet number predicted by  
95 APM directly impacts spectral shape parameter and slope parameter for cloud droplets in the  
96 Morrison 2-mom microphysics scheme and then impacts cloud droplet effective radius, the auto-  
97 conversion of cloud water to rainwater, and ultimately affects the rainwater mass content and  
98 raindrop number concentration.

99 We have carried out WRF-Chem-APM simulations for the period of October 25 – December  
100 31, 2013 at 27 km × 27 km horizontal resolution. The domain covered the main continental United  
101 States, extending approximately from latitudes 21° N to 54° N and from longitudes 62° W to 132°  
102 W, with 180 grid nodes in the east–west direction and 126 in the north–south direction. The model  
103 has 30 vertical layers from the surface to 5 hPa, with finer resolution near the surface (6 layers  
104 within ~1 km above surface). The simulations were restarted on November 1, November 16,  
105 December 1, and December 16, 2013 with continuous chemistry fields from previous runs. The  
106 present analysis focuses on the NEUS during November and December of 2013. Simulated 3-D  
107 fields meteorological, chemical, and aerosol variables were output every three hours for each grid  
108 box and every 15 minutes at the measurement sites described below.

109

## 110 2.2 Measurement site description

### 111 2.2.1. Pinnacle State Park (PSP), Addison, New York (NY)

112 The PSP site is located in Addison, NY, a village in southwestern NY. Its coordinates are  
113 42.09°N and 77.21°W, and it is about 504 meters (m) above sea level (Schwab et al., 2009). The  
114 area surrounding PSP contains a variety of vegetation, including a golf course to the northwest;  
115 forestlands consisting of deciduous and coniferous trees; pastures and fields; and a 50-acre pond  
116 to the site's south (Schwab et al., 2009). The two nearest population centers to PSP are Addison  
117 and Corning. The village of Addison is about 4 km to the northwest of PSP, and it has a population  
118 of approximately 1800 people. The city of Corning is about 15 km to the northeast of PSP, and it  
119 has a population of approximately 11,000 people. Parameters measured include particle number  
120 concentration with a TSI model 3783 CPC, SO<sub>2</sub> with a Thermo model 43i, temperature, relative  
121 humidity, wind speed and direction, solar radiation, and precipitation with calibrated



122 meteorological sensors. These data are collected as minute averages. Gaseous  $\text{NH}_3$  is collected as  
123 part of the AMon network as passive two week samples from the nearby Connecticut Hill site  
124 (NADP, 2018).

125

#### 126 2.2.2. Appalachian State University (APP), Boone, North Carolina (NC)

127 The APP site is located at 1076 m on a hill overlooking the campus of Appalachian State  
128 University (Boone, NC) in the heart of the Southern Appalachian Mountains ( $36.2^\circ$  N,  $81.7^\circ$  W)  
129 (Sherman et al., 2015). The APP site is surrounded by forests in all directions and is not located  
130 near any major highways or major industry. The Charlotte metropolitan area (population 2.5  
131 million) is located approximately 160 km SE of APP and the Piedmont Triangle metropolitan area  
132 (population 1.6 million) is located 200–230 km ESE of APP. Aerosol optical and microphysical  
133 properties are measured as part of NOAA Earth System Research Laboratory (ESRL) (Sherman et  
134 al., 2015).

135

### 136 3. Results

137 WRF-Chem-APM simulated wintertime NPF over the NEUS for the two-month period  
138 (November–December 2013) is examined. The nucleation rate is calculated with a recently  
139 developed  $\text{H}_2\text{SO}_4$ - $\text{H}_2\text{O}$ - $\text{NH}_3$  ternary ion-mediated nucleation (TIMN) scheme (Yu et al., 2018),  
140 which is supported by the detailed CLOUD (Cosmics Leaving Outdoor Droplets) measurements  
141 (Kirkby et al., 2011; Kurten et al., 2016). According to the TIMN scheme,  $\text{H}_2\text{SO}_4$  and  $\text{NH}_3$  are key  
142 nucleation precursors and other parameters such as temperature, relative humidity, ionization rate,  
143 and surface area of pre-existing particles also influence nucleation rates.  $\text{H}_2\text{SO}_4$ , well recognized  
144 to be critical for NPF in the atmosphere, is the oxidation product of  $\text{SO}_2$ . Figure 1 shows the  
145 modeled horizontal spatial distribution for the lower boundary layer (first three model layers,  $\sim 0$   
146 – 400 m above surface) over NEUS during November–December 2013 of the concentrations of  
147 major aerosol precursors (a)  $\text{SO}_2$  & (b)  $\text{H}_2\text{SO}_4$ , and (c)  $\text{NH}_3$ , (d) nucleation rate (J), (e) number  
148 concentration of condensation nuclei  $> 10$  nm (CN10), and (f) number concentration of CCN at  
149 supersaturation 0.4% (CCN0.4). Typical wintertime modeled concentrations of aerosol precursors  
150 in the lower boundary layer over the NEUS are  $[\text{SO}_2] \sim 0.3 - 2$  ppbv,  $[\text{H}_2\text{SO}_4] \sim 0.03 - 0.2$  pptv,  
151 and  $[\text{NH}_3] \sim 0.1 - 5$  ppbv. The modeled spatial distribution of the aerosol precursors is co-located  
152 with their source regions:  $\text{SO}_2$  distribution is in line with the NEI and indicative of coal-fired power



153 plants in the region, especially over the Ohio Valley.  $\text{NH}_3$  hotspots are over emission regions of  
154 agricultural land-use and concentrated animal feeding operations. Calculated monthly mean  
155 nucleation rates in the lower boundary layer range typically from  $\sim 0.1$  to  $\sim 2 \text{ cm}^3\text{s}^{-1}$  over the NEUS  
156 domain and spatial distributions are strongly correlated with concentration of aerosol precursors,  
157 with negligible nucleation over the oceanic area off the east coast. The number concentrations of  
158 CN10 and CCN0.4, calculated from the simulated particle number size distributions, are  $\sim 2000$ –  
159  $7000 \text{ cm}^{-3}$  and  $\sim 100$ – $1000 \text{ cm}^{-3}$ , respectively. Both CN10 and CCN0.4 have highest values over  
160 the Ohio Valley region.

161 To develop further confidence in WRF-Chem-APM simulations, diurnal variations of these  
162 aerosol precursors, as well as meteorological factors are compared with available in situ  
163 measurements for this two-month period at the PSP site in Figure 2. The meteorological parameters  
164 compared are temperature (T) at 2 m above surface, relative humidity (RH), wind direction, solar  
165 radiation, and precipitation in Figure 2 (a–c). Overall, WRF-Chem-APM simulates the diurnal  
166 variations of T and RH in good agreement with measurements (Fig. 3a), with Pearson correlation  
167 coefficient ( $r$ ) of 0.93 for hourly T and 0.74 for hourly RH. The model also captures major changes  
168 in wind direction (Fig. 2b), solar radiation (Fig. 2b), and occurrence of precipitation (Fig. 2c). The  
169 model slightly over-predicted RH and T. It should be noted that RH measurements were taken at  
170 2 m above surface while modeled RH is the average of model surface layer ( $\sim 0$ – $100$  m). The  
171 differences/deviations during some days can also be associated with model uncertainties and sub-  
172 grid variations within the  $27 \text{ km} \times 27 \text{ km}$  grid box. In situ measurements of  $[\text{SO}_2]$  and  $[\text{NH}_3]$  from  
173 the PSP site are used to examine their simulated values. Absolute values of  $[\text{SO}_2]$  and their day-  
174 to-day variations (from below 0.1 ppbv to above 1 ppbv) are overall consistent with observations  
175 (Fig. 2c), with  $r$  of 0.48 and mean bias error (MBE) of  $-12\%$ . The daily variation of  $[\text{NH}_3]$  (Fig.  
176 2d) is more dramatic than that of  $[\text{SO}_2]$ , with the maximum value reaching  $\sim 10$  ppbv on Day 320  
177 and minimum value approaching zero on many days. In WRF-Chem,  $[\text{NH}_3]$  is calculated with  
178 ISOROPIA II (Fountoukis and Nenes, 2007) and assumes equilibrium between gaseous and  
179 particulate phases. In addition to emission, deposition, and transport,  $[\text{NH}_3]$  is also controlled by  
180 particle compositions and temperature. The best available  $[\text{NH}_3]$  data for the site during this period  
181 is from the Ammonia Monitoring Network (AMoN), which provides 2-week averages. The  
182 average values of modeled (observed)  $[\text{NH}_3]$  during November and December are 0.26 (0.5) and  
183 0.04 (0.2) ppbv, respectively, indicating average model–observation consistency with lower bias



184 of model simulations. Measurements of  $[\text{NH}_3]$  at high temporal resolution are apparently needed  
185 to more rigorously evaluate the model performance.

186 During this wintertime period, biogenic emissions are low, leading to negligible modeled  
187 isoprene and monoterpene (not shown) and [LV-SOG] (Fig. 2d, generally  $< 10^6 \text{ cm}^{-3}$ ). In contrast,  
188 the peak  $[\text{H}_2\text{SO}_4]$  can reach above  $10^7 \text{ cm}^{-3}$ . As a result of its sole production from photochemistry  
189 and its short lifetime associated with condensation on pre-existing particles,  $[\text{H}_2\text{SO}_4]$  shows strong  
190 diurnal variation.  $[\text{H}_2\text{SO}_4]$  above  $\sim 3 \times 10^6 \text{ cm}^{-3}$  is a necessary condition for substantial nucleation  
191 (with nucleation rate  $J > 0.1 \text{ cm}^{-3} \text{ s}^{-1}$ ) to occur (Fig. 2e). On Days 319 and 320 (November 15-16),  
192 peak  $[\text{H}_2\text{SO}_4]$  was above  $3 \times 10^7 \text{ cm}^{-3}$  and maximum nucleation rate reached up to  $10 \text{ cm}^{-3} \text{ s}^{-1}$ . In  
193 addition to  $[\text{H}_2\text{SO}_4]$ , which also depends on surface area of pre-existing particles (and hence RH),  
194  $[\text{NH}_3]$  and T are other two important parameters controlling the variations of nucleation rates. It  
195 should be noted that ionization rates assumed in the model, while also important for NPF under  
196 the conditions, do not have much temporal and horizontal variations. The variations of  $J$  lead to  
197 large changes of CN10, from several hundreds to above tens of thousands per  $\text{cm}^{-3}$ , which is in  
198 good agreement with observations (Fig. 2e) and analyzed in more detail in Figure 3.

199 Figure 3 presents simulated surface-level (model first layer) particle number size distributions  
200 (PNSD), and CN10, and CCN0.4 during the two-month period for two sites in NEUS where CN10  
201 in situ measurements are available: (a) PSP and (b) APP. The evolution of PNSD shows clearly the  
202 occurrence of strong nucleation and growth events on some days leading to significant increase in  
203 CN10 and CCN0.4. During the winter months, photochemistry is relatively weak and biogenic  
204 emissions are small. Nevertheless, our model simulations show that nucleated particles of a few  
205 nanometers, through  $\text{H}_2\text{SO}_4$  condensation and equilibrium uptake of  $\text{HNO}_3$ ,  $\text{NH}_3$ , and  $\text{H}_2\text{O}$ , are  
206 able to grow to 10–30 nm on most of nucleation event days and even to 60–100 nm particles that  
207 can act as CCN during some of these days. The model captures quite well the absolute values of  
208 CN10 ( $\sim 200 - 20000 \text{ cm}^{-3}$ ) as well as their daily variability at both sites, with MBE=9%, 6% and  
209  $r = 0.70, 0.55$  for the PSP and APP site, respectively. The PNSDs and CN10 time series indicate  
210 that at both sites, CN10 is dramatically elevated (by a factor of up to  $\sim 10$ ) in the aftermath of  
211 nucleation events. CN10 associated with primary particles (CN10\_PP, mainly black carbon and  
212 primary organic carbon, with coating of secondary species) remains fairly constant ( $\sim 100 \text{ cm}^{-3}$ )  
213 during nucleation events. Based on the model simulation, the mean CN10 (CN10\_PP) during the  
214 two month period are  $2989 (106) \text{ cm}^{-3}$  for the PSP site and  $3180 (88) \text{ cm}^{-3}$  for the APP site, showing





215 that the secondary particles (CN10 – CN10\_PP) account for >95% of total CN10. The  
216 concentration of CCN0.4 and the fraction associated with secondary particles ( $f_{\text{CCN\_SP}}$ ) in the  
217 surface layer at the two sites have large variations, ranging from several tens to several thousand  
218 per  $\text{cm}^{-3}$  for CCN0.4 and  $\sim 0$ –90% for  $f_{\text{CCN\_SP}}$ . CCN0.4 and  $f_{\text{CCN\_SP}}$  are generally elevated during  
219 nucleation event days.

220 For detailed examination of the contribution of nucleation to CCN0.4 at the regional scale, a  
221 four-day period (November 15–18, 2013, marked within a black rectangle in Fig. 3) is selected so  
222 as to have all permutations of nucleation events and non-events at the two sites (PSP and APP).  
223 November 15 (Day 319) has nucleation events at both sites, November 16 has nucleation event  
224 only at PSP, November 17 has nucleation non-events at both sites, and November 18 has nucleation  
225 event only at APP. Figure 4 shows for the NEUS, containing the PSP and APP sites, the modeled  
226 horizontal spatial distribution of  $[\text{SO}_2]$ ,  $[\text{H}_2\text{SO}_4]$ , and nucleation rate ( $J$ ) averaged within the  
227 boundary layer (first 7 model layers above surface).  $[\text{SO}_2]$  is controlled by emission, transport,  
228 chemistry, and deposition. Large daily variation of  $[\text{SO}_2]$  in the NEUS and the important role of  
229  $\text{SO}_2$  emission from Ohio Valley region can be clearly seen in Fig. 4. The dependence of nucleation  
230 rate on  $[\text{H}_2\text{SO}_4]$ , which is determined by  $\text{SO}_2$  oxidation production rate and condensation sink, is  
231 clear over the NEUS. Consistent with the nucleation events and non-events observed at PSP and  
232 APP sites during the 4-day period as shown in Fig. 3, Figure 4 shows that the nucleation is  
233 generally at the regional scale with spatial distribution similar to that of  $[\text{H}_2\text{SO}_4]$ . These regional  
234 wintertime nucleation events contribute significantly to CCN0.4 in the NEUS as evidenced in the  
235 day-to-day spatial variations in CCN0.4 given in Fig. 5 (upper panels). Regions of high CCN0.4,  
236 generally dominated by secondary particles (Fig. 5 middle panes), correspond well with areas of  
237 high nucleation (Fig. 4, lower panels)). More than  $\sim 80\%$  of CCN0.4 is of secondary origin in  
238 regions with CCN0.4 above  $\sim 1000 \text{ cm}^{-3}$ . Figure 5 (lower panels) also gives daily mean Cloud  
239 Droplet Number Concentration (CDNC) in the boundary layer (liquid water content weighted  
240 average) during the period. Apparently, clouds formed in regions of higher CCN0.4 have larger  
241 CDNC and secondary particles contribute to CDNC in these regions, highlighting the need for  
242 better representation of secondary particle formation and growth in regional models.

243 So far, our analysis focuses on aerosol and precursors near surface or in the boundary layer. To  
244 examine the vertical variations, Figure 6 shows the two-month (November–December 2013) mean  
245 nucleation rates and consequent contribution to CN10 (SP fraction,  $f_{\text{CN10\_SP}}$ ) and CCN0.4 (SP





246 fraction,  $f_{\text{CCN}_{0.4}}^{\text{SP}}$ ) in the lower boundary layer (below  $\sim 960$  mb), lower troposphere ( $\sim 960$ – $800$   
247 mb), middle troposphere ( $\sim 800$ – $470$  mb), and upper troposphere ( $\sim 470$ – $250$  mb) over the NEUS.  
248 The model simulations indicate substantial nucleation at all altitudes although nucleation rates are  
249 higher in lower boundary layer and upper troposphere. Horizontal distributions of nucleation rates  
250 in lower boundary layer and lower troposphere differ significantly from those in middle and upper  
251 troposphere, indicating quite different sources of air mass and that the influence of local emission  
252 is limited to the lower troposphere. Secondary particles dominate CN10 at all altitudes over NEUS  
253 and  $f_{\text{CN}_{10}}^{\text{SP}}$  increases with altitudes from  $>\sim 85\%$  in lower boundary layer to  $>\sim 95\%$  in the upper  
254 troposphere. In the lower boundary layer, secondary particles formed via nucleation contribute to  
255 the CCN0.4 number concentration from about 20–30% over the New England region to  $\sim 40$ – $50\%$   
256 over the Ohio Valley region. Similar to that of CN10, the SP fraction of CCN0.4 increases with  
257 altitudes, reaching to 50–60% in the middle troposphere and 70–85% in the upper troposphere  
258

#### 259 **4. Summary**

260 New particle formation (NPF) has been well recognized as an important source of ultrafine  
261 particles which can lead to adverse health impacts and CCN which affects cloud, precipitation, and  
262 climate. In this study, wintertime particle formation over the Northeastern United States (NEUS)  
263 and its contribution to particle number concentrations and CCN are investigated. Wintertime NPF  
264 in NEUS is expected to be dominated by inorganic species as a result of very low biogenic  
265 emissions. Based on WRF-Chem-APM simulations for a two-month period (November–  
266 December 2013) and comparisons with measurements, we show that substantial regional scale  
267 NPF occurs in the winter over NEUS despite weaker photochemistry and low biogenic emissions.  
268 The recently developed physics-based  $\text{H}_2\text{SO}_4$ - $\text{H}_2\text{O}$ - $\text{NH}_3$  ternary ion-mediated nucleation scheme  
269 appears to be able to capture the absolute values of particle number concentrations as well as their  
270 daily variations observed at two sites in NEUS. The freshly nucleated nanometer particles can  
271 grow to 10–30 nm on most nucleation event days and to CCN sizes during some of these days.  
272 CN10 and CCN0.4 are dramatically elevated in the aftermath of nucleation events. Calculated  
273 monthly mean nucleation rates in the boundary layer over the NEUS range from  $\sim 0.1$  to  $\sim 2$   $\text{cm}^3\text{s}^{-1}$   
274  $^1$  and spatial distributions are strongly correlated with concentration of aerosol precursors. The  
275 monthly mean number concentrations of CN10 and CCN0.4 are around 2000–7000  $\text{cm}^{-3}$  and 100–  
276 1000  $\text{cm}^{-3}$ , respectively. Both CN10 and CCN0.4 have highest values over the Ohio Valley region,



277 a key source region of anthropogenic SO<sub>2</sub>. The model simulations indicate substantial nucleation  
278 occurs at all altitudes although nucleation rates are higher in lower boundary and upper troposphere.  
279 Secondary particles dominate CN10 at all altitudes over NEUS and its fraction increases with  
280 altitudes from >~85% near surface to >~95% in upper troposphere. The fraction of CCN0.4 due  
281 to secondary particles also increases with altitudes, from 20-50% in the lower boundary layer to  
282 50-60% in the middle troposphere and 70–85% in the upper troposphere.

283

284 **Data availability.** The model output and observational data used for comparison are available on  
285 request from the authors.

286 **Author contributions.** FY, GL, and YZ developed the project idea. GL and FY updated the model  
287 and carried out the numerical simulations. FY and AN wrote the paper, with contribution from GL  
288 and JJS. JJS and JBS contributed observational data used in the comparison.

289 **Competing interests.** The authors declare that they have no conflict of interest.

290 **Acknowledgements:** This study was supported by NYSERDA under contract 100416 and NSF  
291 under grants OISE-1545917 and AGS-1550816, and. Ammonia Monitoring Network (AMoN)  
292 data used for comparison is from National Atmospheric Deposition Program (NRSP-3), 2017,  
293 NADP Program Office, Illinois State Water Survey, University of Illinois, Champaign, IL 61820  
294 (<http://nadp.sws.uiuc.edu/AMoN/>).

## 295 **References**

- 296 Abdul-Razzak, H., and Ghan, S. J., A parameterization of aerosol activation, 3, Sectional  
297 representation, *J. Geophys. Res.*, 107( D3), doi:10.1029/2001JD000483, 2002.
- 298 Charlson R. J., Schwartz S. E., Hales J. M., Cess R. D., Coakley J. A., Jr., Hansen J. E. and  
299 Hofmann D. J. Climate forcing by anthropogenic aerosols. *Science* 255, 423-430, 1992.
- 300 Clough, S. A., M. W. Shephard, E. J. Mlawer, J. S. Delamere, M. J. Iacono, K. Cady-Pereira, S.  
301 Boukabara, and P. D. Brown, Atmospheric radiative transfer modeling: A summary of the  
302 AER codes, *J. Quant. Spectrosc. Radiat. Transfer*, 91, 233–244,  
303 doi:10.1016/j.jqsrt.2004.05.058, 2005.
- 304 Fountoukis, C., and A. Nenes, ISORROPIA II: A computationally efficient thermodynamic  
305 equilibrium model for K<sup>+</sup>-Ca<sup>2+</sup>-Mg<sup>2+</sup>-NH<sub>4</sub><sup>+</sup>-Na<sup>+</sup>-SO<sub>4</sub><sup>2-</sup>-NO<sub>3</sub><sup>-</sup>-Cl<sup>-</sup>-H<sub>2</sub>O aerosols, *Atmos.*



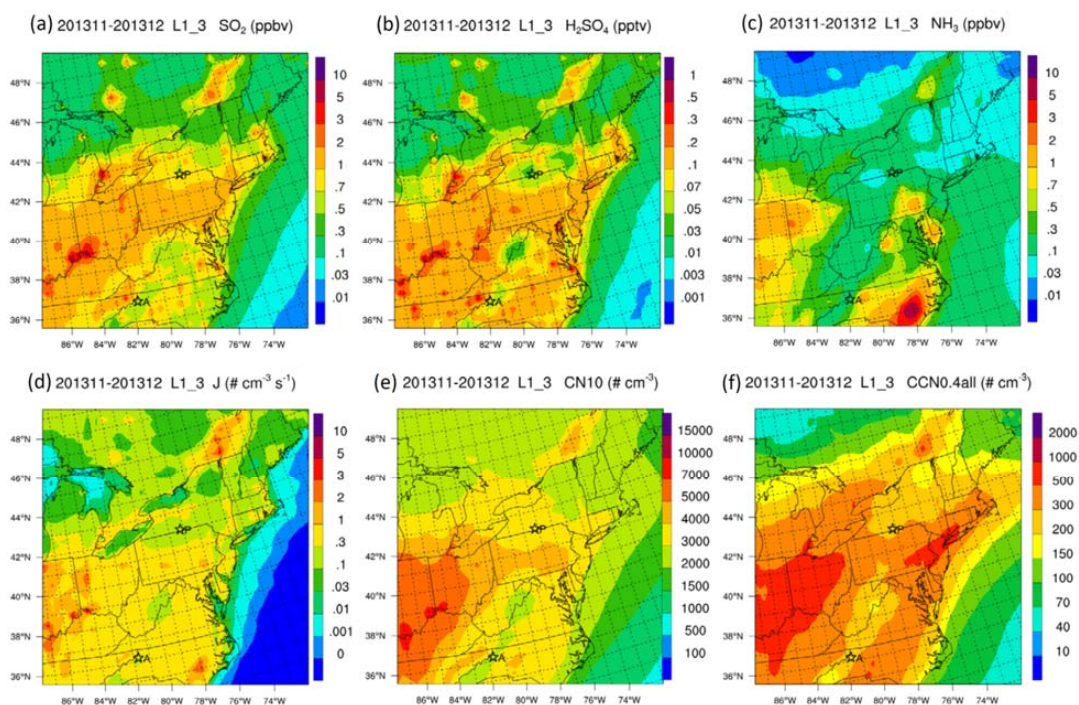
- 306 Chem. Phys.,7(17), 4639–4659, doi:10.5194/acp-7-4639-2007, 2007.
- 307 Gaudet, L. C., K. J. Sulia, F. Yu, and G. Luo, Sensitivity of Lake-Effect Cloud Microphysical  
308 Processes to Ice Crystal Habit and Nucleation during OWLeS IOP4, *J. of Climate*,  
309 <https://doi.org/10.1175/JAS-D-19-0004.1>, 2019.
- 310 Grell, G. A. and Freitas, S. R.: A scale and aerosol aware stochastic convective parameterization  
311 for weather and air quality modeling, *Atmos. Chem. Phys.*, 14, 5233-5250,  
312 <https://doi.org/10.5194/acp-14-5233-2014>, 2014.
- 313 Grell, G. A., Peckham, S. E., McKeen, S., Schmitz, R., Frost, G.,Skamarock, W. C., and Eder, B.:  
314 Fully coupled “online” chem-istry within the WRF model, *Atmosph. Env.*, 39, 6957–  
315 6975,2005.
- 316 Guenther, A., Karl, T., Harley, P., Wiedinmyer, C., Palmer, P. I., and Geron, C.: Estimates of  
317 global terrestrial isoprene emissions using MEGAN (Model of Emissions of Gases and  
318 Aerosols from Nature), *Atmos. Chem. Phys.*, 6, 3181-3210, [https://doi.org/10.5194/acp-6-](https://doi.org/10.5194/acp-6-3181-2006)  
319 3181-2006, 2006.
- 320 Han, Y., T. Zhu, T. Guan, Y. Zhu, J Liu, Y. Ji, S. Gao, F. Wang, H. Lu, W. Huang, Association  
321 between size-segregated particles in ambient air and acute respiratory inflammation, *Science*  
322 of The Total Environment, 565, 412-419, 2016.
- 323 Hong, S.-Y., Noh, Y., Dudhia, J., A new vertical diffusion package with an explicit treatment of  
324 entrainment processes. *Mon. Weather Rev.* 134 (9), 2318–2341, 2006.
- 325 Kirkby, J. and co-authors, Role of sulphuric acid, ammonia and galactic cosmic rays in  
326 atmospheric aerosol nucleation, *Nature*, 476, 429–433, 2011.
- 327 Knibbs, L.D., Cole-Hunter, T., Morawska, L., A review of commuter exposure to ultrafine particles  
328 and its health effects. *Atmos. Environ.* 45, 2611-2622.  
329 <http://dx.doi.org/10.1016/j.atmosenv.2011.02.065>, 2011
- 330 Kürten, A., Bergen, A., Heinritzi, M., Leiminger, M., Lorenz, V., Piel, F., Simon, M., Sitals, R.,  
331 Wagner, A. C., and Curtius, J.: Observation of new particle formation and measurement of  
332 sulfuric acid, ammonia, amines and highly oxidized organic molecules at a rural site in central  
333 Germany, *Atmos. Chem. Phys.*, 16, 12793–12813, <https://doi.org/10.5194/acp-16-12793-2016>,  
334 2016.
- 335 Lee, S.-H., Gordon, H., Yu, H., Lehtipalo, K., Haley, R., Li, Y., and Zhang, R.: New particle  
336 formation in the atmosphere: From molecular clusters to global climate, *J. Geophys. Res.*, 124,



- 337 <https://doi.org/10.1029/2018JD029356>, 2019.
- 338 Luo, G., and F. Yu, Simulation of particle formation and number concentration over the Eastern  
339 United States with the WRF-Chem + APM model, *Atmos. Chem. Phys.*, 11, 11521-11533,  
340 doi:10.5194/acp-11-11521-2011, 2011.
- 341 Morrison, H., G. Thompson, and V. Tatarskii, Impact of cloudmicrophysics on the development  
342 of trailing stratiform precipitation in a simulated squall line: Comparison of one- and two-  
343 moment schemes, *Mon. Weather Rev.*, 137, 991–1007, doi:10.1175/2008MWR2556.1, 2009.
- 344 NADP, National Atmospheric Deposition Program 2017 Annual Summary. Wisconsin State  
345 Laboratory of Hygiene, University of Wisconsin-Madison, WI. Available at:  
346 <http://nadp.slh.wisc.edu/lib/dataReports.aspx>, 2018
- 347 Pierce, J. R. and Adams, P. J.: Uncertainty in global CCN concentrations from uncertain aerosol  
348 nucleation and primary emission rates, *Atmos. Chem. Phys.*, 9, 1339–1356, doi:10.5194/acp-  
349 9-1339-2009, 2009.
- 350 Schell B., I.J. Ackermann, H. Hass, F.S. Binkowski, and A. Ebel, Modeling the formation of  
351 secondary organic aerosol within a comprehensive air quality model system, *Journal of*  
352 *Geophysical research*, 106, 28275-28293, 2001.
- 353 Schwab, J.J.; Spicer, J.B.; Demerjian, K.L. Ozone, Trace Gas, and Particulate Matter  
354 Measurements at a Rural Site in Southwestern New York State: 1995-2005. *J. Air Waste*  
355 *Manage. Assoc.* 59, 293 – 309, doi: 10.3155/1047-3289.59.3.293, 2009.
- 356 Sherman, J.P., P.J. Sheridan, J.A. Ogren, E.A. Andrews, L. Schmeisser, A. Jefferson, and S.  
357 Sharma, A multi-year study of lower tropospheric aerosol variability and systematic  
358 relationships from four North American regions, *Atmos. Chem. Phys.*, 15, 12487-12517,  
359 doi:10.5194/acp-15-12487-2015, 2015.
- 360 Spracklen, D., Carslaw, K., Kulmala, M., Kerminen, V.-M., Sihto, S.-L., Riipinen, I., Merikanto,  
361 J., Mann, G., Chipperfield, M., Wiedensohler, A., Birmili, W., and Lihavainen,  
362 H.: Contribution of particle formation to global cloud condensation nuclei concentrations,  
363 *Geophys. Res. Lett.*, 35, L06808, doi:10.1029/2007GL033038, 2008.
- 364 Twomey, S., 1977: The Influence of Pollution on the Shortwave Albedo of Clouds. *J. Atmos. Sci.*,  
365 34, 1149–1152, <https://doi.org/10.1175/1520-0469>, 1977.
- 366 Yarwood, G., S. Rao, M. Yocke, and G.Z. Whitten, Updates to the Carbon Bond Mechanism:  
367 CB05. US EPA Final Report, 161 pp., 2005. [Available at



368 [http://www.camx.com/publ/pdfs/CB05\\_Final\\_Report\\_120805.pdf](http://www.camx.com/publ/pdfs/CB05_Final_Report_120805.pdf)  
369 Yu, F. and Luo, G.: Simulation of particle size distribution with a global aerosol model:  
370 contribution of nucleation to aerosol and CCN number concentrations, *Atmos. Chem. Phys.*,  
371 9, 7691-7710, <https://doi.org/10.5194/acp-9-7691-2009>, 2009.  
372 Yu, F., A secondary organic aerosol formation model considering successive oxidation aging and  
373 kinetic condensation of organic compounds: global scale implications, *Atmos. Chem. Phys.*,  
374 11, 1083-1099, doi:10.5194/acp-11-1083-2011, 2011.  
375 Yu, F., G. Luo, and X. Ma, Regional and global modelling of aerosol optical properties with a size,  
376 composition, and mixing state resolved particle microphysics model, *Atmos. Chem. Phys.*, 12,  
377 5719-5736, doi:10.5194/acp-12-5719-2012, 2012.  
378 Yu, F., Luo, G., Pryor, S. C., Pillai, P. R., Lee, S. H., Ortega, J., Schwab, J. J., Hallar, A. G.,  
379 Leaitch, W. R., Aneja, V. P., Smith, J. N., Walker, J. T., Hogrefe, O., and Demerjian, K. L.:  
380 Spring and summer contrast in new particle formation over nine forest areas in North America,  
381 *Atmos. Chem. Phys.*, 15, 13993-14003, doi:10.5194/acp-15-13993-2015, 2015.  
382 Yu, F., Nadykto, A. B., Herb, J., Luo, G., Nazarenko, K. M., and Uvarova, L. A.: H<sub>2</sub>SO<sub>4</sub>-H<sub>2</sub>O-  
383 NH<sub>3</sub> ternary ion-mediated nucleation (TIMN): Kinetic-based model and comparison with  
384 CLOUD measurements, *Atmos. Chem. Phys.*, 18, 17451-17474, [https://doi.org/10.5194/acp-](https://doi.org/10.5194/acp-18-17451-2018)  
385 [18-17451-2018](https://doi.org/10.5194/acp-18-17451-2018), 2018.  
386  
387  
388

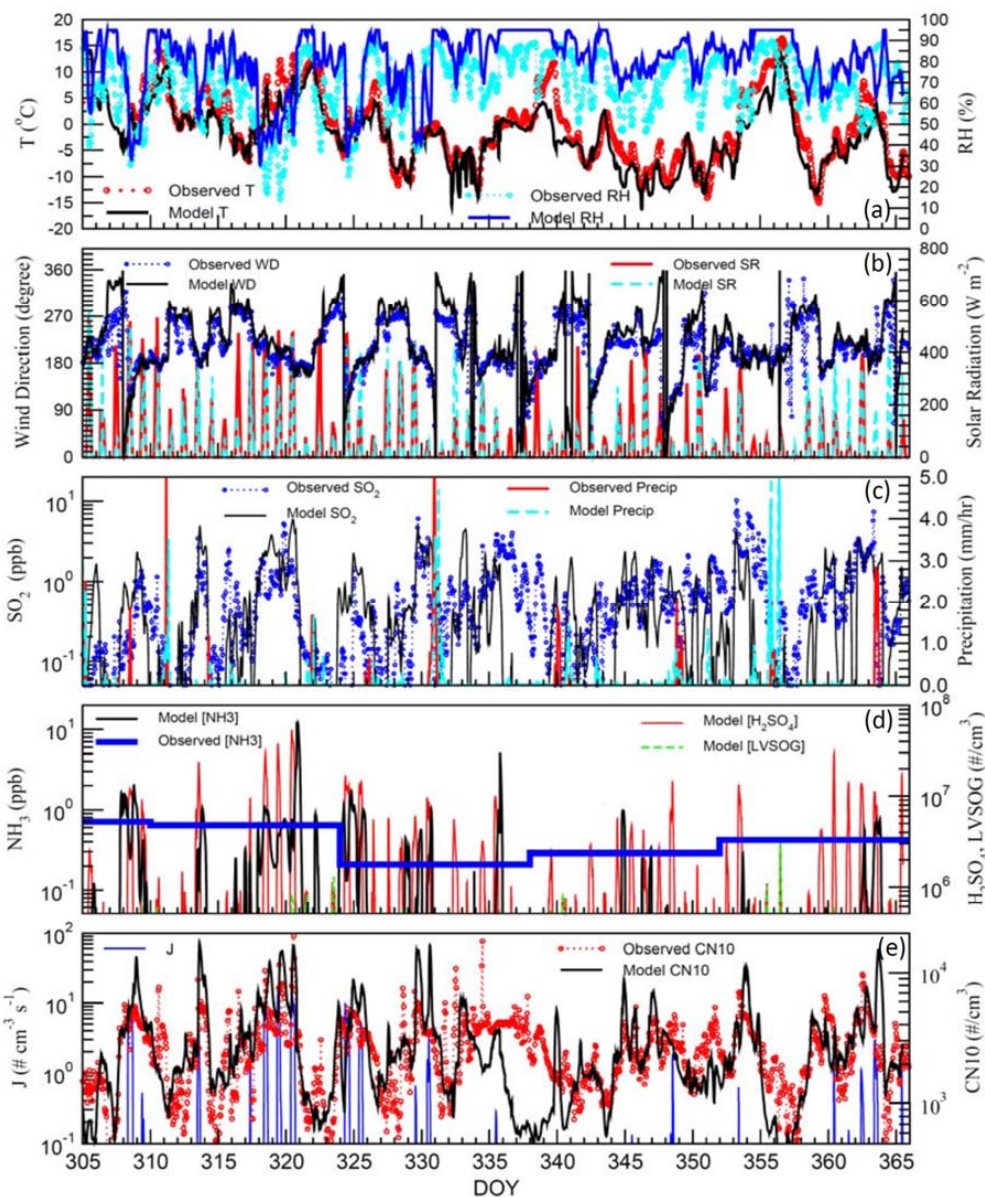


389

390 **Figure 1.** Horizontal spatial distribution of WRF-Chem-APM simulated average wintertime (2013  
391 November–December) (a) [SO<sub>2</sub>], (b) [H<sub>2</sub>SO<sub>4</sub>], (c) [NH<sub>3</sub>], (d) nucleation rate (*J*), (e) number  
392 concentration of condensation nuclei > 10 nm (CN10), and (f) cloud condensation nuclei at  
393 supersaturation 0.4% (CCN0.4) in the lower boundary layer (~ 0 – 400 m above surface, first three  
394 model layers) over the Northeastern United States (NEUS). Measurement sites Appalachian State  
395 University (APP), North Carolina (A) and Pinnacle State Park (P), New York are marked on the  
396 maps.

397





398

399 **Figure 2.** Modeled diurnal variability of wintertime (November–December 2013) (a) temperature  
400 (T) and relative humidity (RH), (b) wind direction (WD) and solar radiation (SR), (c) [SO<sub>2</sub>] and  
401 precipitation, (d) [NH<sub>3</sub>], [H<sub>2</sub>SO<sub>4</sub>], and concentration of low-volatile secondary organic gas ([LV-  
402 SOG]), and (e) nucleation rate (*J*) and CN10 at the Pinnacle State Park (PSP) site compared with  
403 in situ measurements. X-axis is the day of year (DOY).



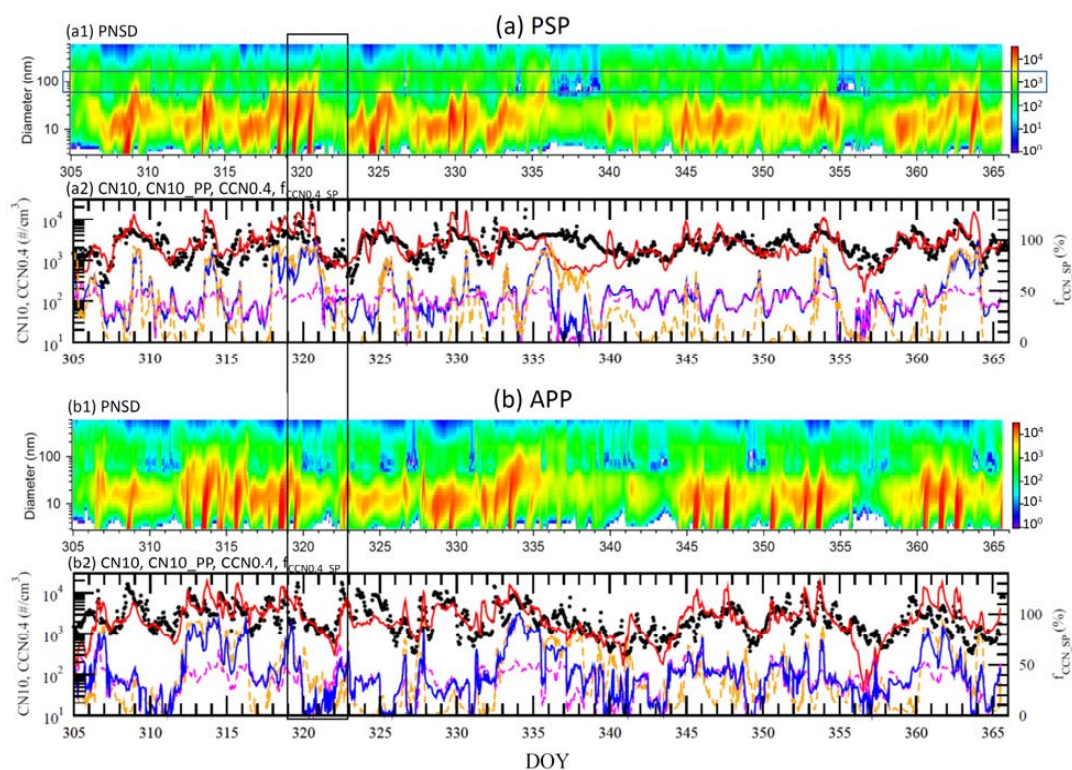


**Figure 3.** For the (a) PSP and (b) APP sites in the NEUS: Modeled wintertime (November–December 2013) evolution of particle number size distributions (PNSD, a1, b1), and time series (a2, b2) of CN10 (red line), CN10 due to primary particles (CN10\_PP, dashed magenta line), CCN0.4 (blue line), and percentage of CCN0.4 associated with secondary particles ( $f_{CCN\_SP}$ , dashed orange line). In a2 and b2, CN10 values from observations (black circles) are also shown for comparison. The model results are for the model surface layer ( $\sim 0$ –100 m above surface). Selected 4-day period from November 15–18, 2013 with nucleation events and non-events is marked within a black rectangle.

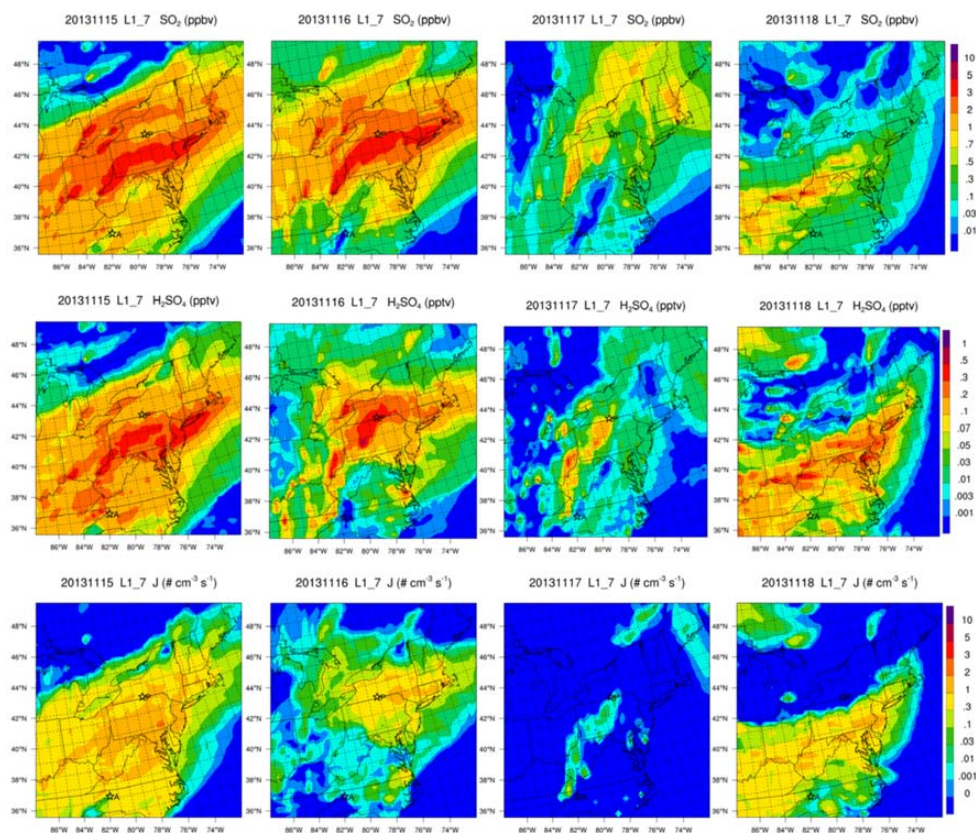


**Figure 4.** For the each of the 4-day period from (left to right) November 15–18, 2013: (top to bottom) modeled horizontal spatial distribution of  $[\text{SO}_2]$ ,  $[\text{H}_2\text{SO}_4]$ , and nucleation rate ( $J$ ) over the NEUS, with the measurement sites Pinnacle State Park (P) and APP (A) marked on the maps.

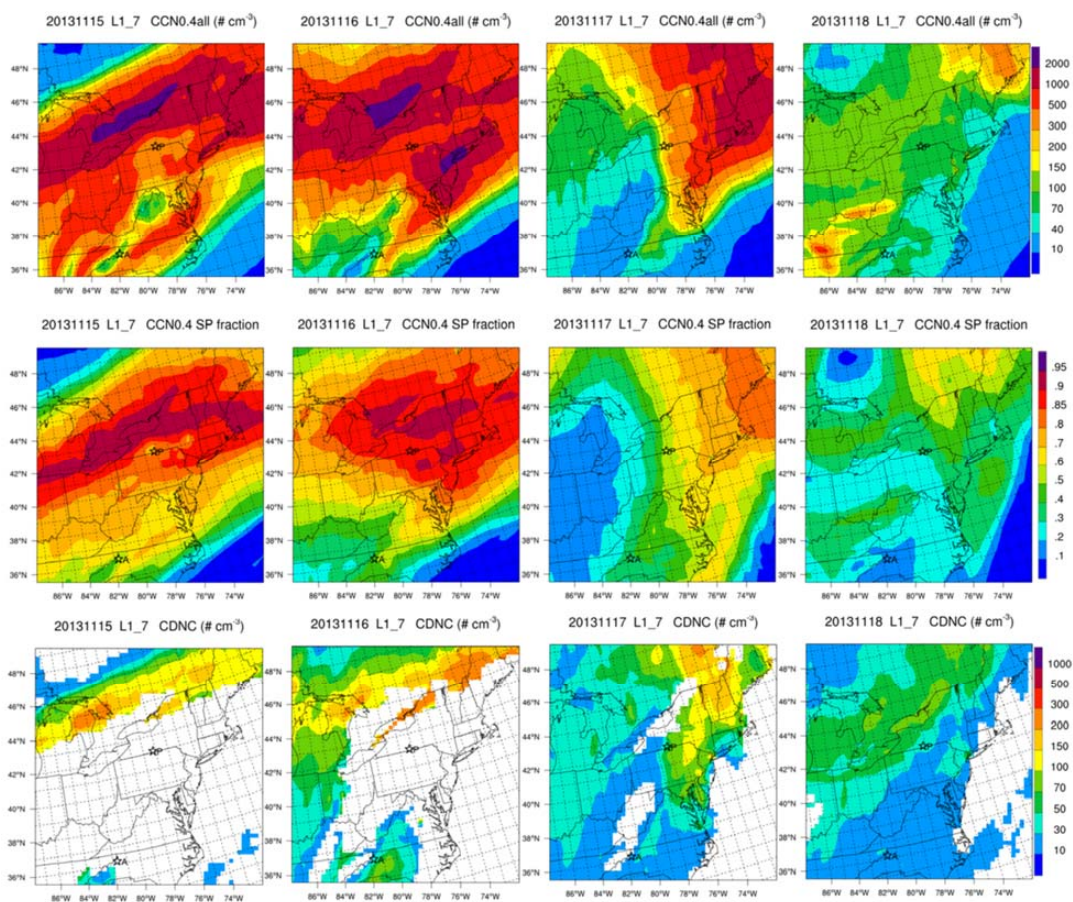


**Figure 5.** For the each of the 4-day period from (left to right) November 15–18, 2013: (top) CCN0.4 and (middle) its secondary particle fraction (CCN0.4 SP), and (bottom) cloud droplet (CDNC) modeled horizontal spatial distribution over the NEUS, with the measurement sites Pinnacle State Park (P) and APP (A) marked on the maps.



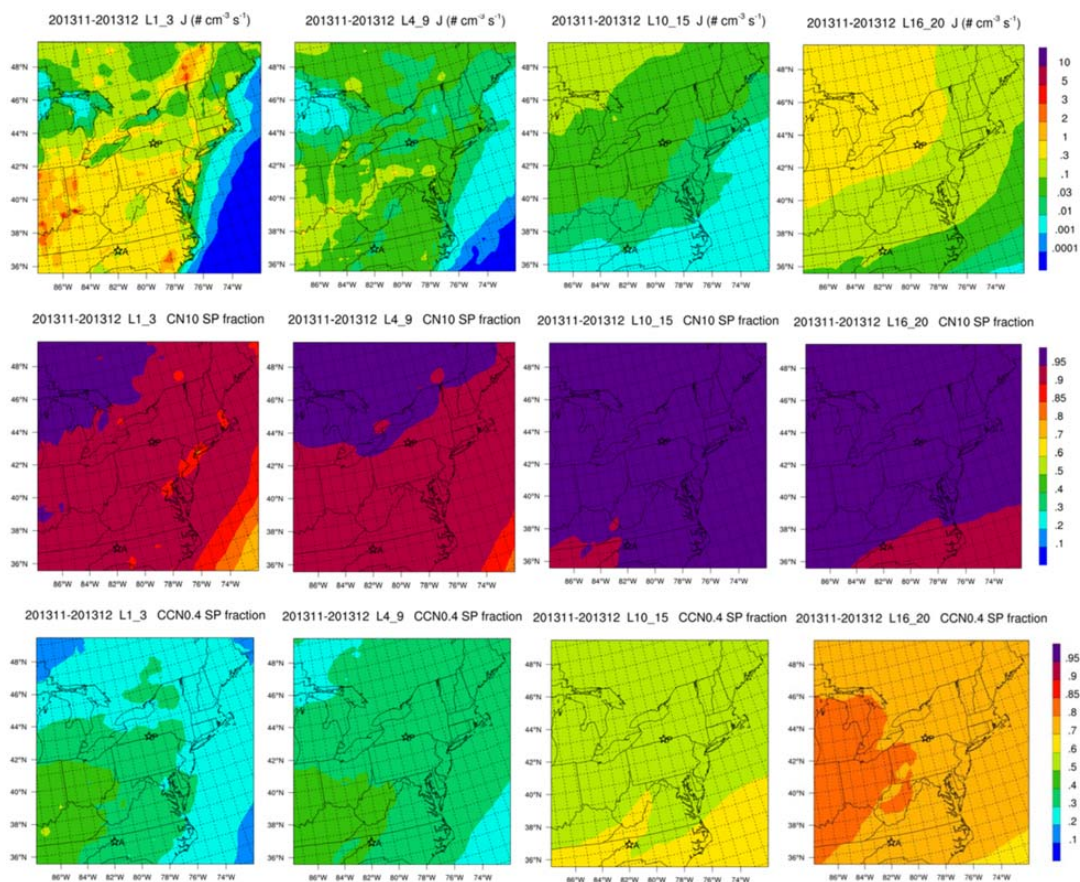


**Figure 6.** Modeled average wintertime (2013 November–December) (top) nucleation rate ( $J$ ), (bottom) CN SP fraction, and (bottom) CCN0.4 SP fraction for (left to right) the surface layer, lower, middle, and upper troposphere.